



LETTER

Drifting patterns as field reversals

To cite this article: F. Pétrélis *et al* 2015 *EPL* **112** 54007

View the [article online](#) for updates and enhancements.

Related content

- [Instabilities on a turbulent background](#)
Stéphan Fauve, Johann Herault,
Guillaume Michel et al.
- [Chaotic dynamics of the magnetic field
generated by dynamo action in a
turbulent flow](#)
F Pétrélis and S Fauve
- [Bifurcations of a large-scale circulation in a
quasi-bidimensional turbulent flow](#)
G. Michel, J. Herault, F. Pétrélis et al.

Drifting patterns as field reversals

F. PÉTRÉLIS, C. LAROCHE, B. GALLET and S. FAUVE

Laboratoire de Physique Statistique, Ecole Normale Supérieure, CNRS, Université P. et M. Curie, Université Paris Diderot - Paris, France

received 21 September 2015; accepted in final form 11 December 2015

published online 23 December 2015

PACS 47.35.-i – Hydrodynamic waves

PACS 47.10.Fg – Dynamical systems methods

Abstract – One-dimensional patterns generated by the Faraday instability at the surface of a vertically vibrated fluid are investigated when the reflection symmetry in the direction of the pattern is broken. For large symmetry breaking, the stationary instability turns into a Hopf bifurcation at a codimension-2 point. This Hopf bifurcation amounts to a periodic drift of the pattern. Further above the onset of the instability, this drift transition competes with the Eckhaus instability as predicted by the study of a model built upon the Swift-Hohenberg equation. In the presence of noise, the drift becomes random and time series of the pattern amplitude display random reversals (sign changes). We show that these reversals belong to the same class as those observed in a variety of contexts such as magnetic fields generated by dynamo action.

Copyright © EPLA, 2015

Introduction. – There exist several examples of field reversals in geophysical or astrophysical fluid dynamics. The most striking one is provided by the Earth magnetic field that displays random reversals during which the axial dipole component vanishes and changes sign. Another example is the magnetic field of the Sun that changes polarity almost periodically, roughly every 11 years [1]. Besides these examples from magnetohydrodynamics, there exist purely hydrodynamic systems in which reversals of a large-scale velocity occur on a turbulent background. One of them is the quasi-biennial oscillation: the zonal wind in the equatorial stratosphere of the Earth flips from eastward to westward with a period of roughly two years but unlocked to any seasonal cycle [2]. Other examples have been studied in several laboratory experiments or using numerical simulations: random reversals of the large-scale circulation in turbulent Rayleigh-Bénard convection [3] or in Kolmogorov-type flows, *i.e.* quasi-two-dimensional turbulent flows driven by a spatially periodic forcing [4]. Reversals of the magnetic field have also been studied in a laboratory experiment [5] and modeled in the framework of the low-dimensional dynamical system theory [6].

Field reversals correspond to trajectories that connect two symmetric states in the phase space of the system. In the case of the magnetic field, the equations of magnetohydrodynamics (MHD) are invariant under the transformation ($\mathbf{v} \rightarrow \mathbf{v}, \mathbf{B} \rightarrow -\mathbf{B}$) where \mathbf{v} is the velocity field and \mathbf{B} the magnetic field. This symmetry is broken at the dynamo threshold, where the magnetic field is spontaneously

generated by the motion of an electrically conducting fluid. Convection rolls, and the large-scale circulations involved in the QBO or in Kolmogorov flows can also be generated with both signs at their instability threshold. In all these examples, the broken symmetry at instability threshold is then statistically restored in a regime with periodic or random reversals. It has been commonly believed that random reversals are generated by turbulent velocity fluctuations that induce transitions from one state to the symmetric one as for a particle subjected to noise in a double-well potential. Obviously, time periodic reversals cannot be described in this framework. In addition, reversal dynamics never correspond to a homogeneous decay of the field then growing again with the opposite polarity. Some components decay first, some others are generated during the reversal process such that reversals correspond to complex trajectories in phase space. It is rather unlikely that turbulent fluctuations act coherently during this whole process and in the whole flow volume. Then, there should exist some trajectories in phase space that are, either constrained by the deterministic part of the dynamics, or are more likely to occur if induced by fluctuations. The problem is to determine these easiest paths that are followed during reversals.

When the field is a spatially periodic pattern along the x -axis, the easy paths for reversals can be found immediately; they correspond to spatial translations of the pattern by half a wavelength. For a system of infinite extent close to the pattern-forming instability threshold,

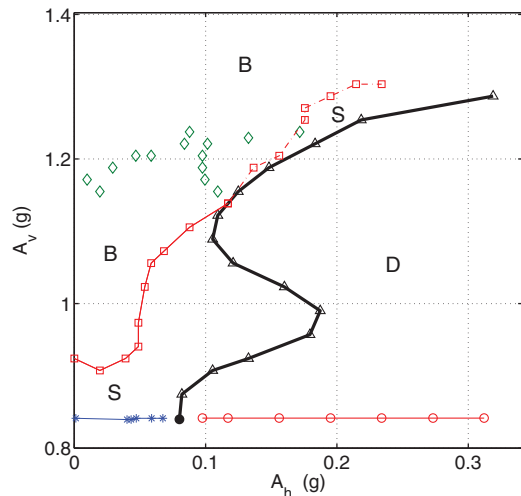


Fig. 1: (Color online) Parameter space: vertical *vs.* horizontal acceleration (A_h, A_v). Symbols indicate the onset of bifurcations between different regimes. For $A_v \leq A_{vc} \simeq 0.85g$, the flat surface is stable. For $A_h \leq A_{h2} \simeq 0.08g$, blue asterisks indicate the onset of the Faraday instability that generates a stationary pattern of subharmonic instability. For larger A_h , red circles correspond to the onset of the Hopf bifurcation toward the drifting regime. The full black circle is the codimension-2 point. At larger A_v , black triangles indicate the saddle-node bifurcation from the stationary to the drift regime. Above the empty squares, the system is bistable, with two stationary solutions. For $A_h = 0$, this bistability corresponds to the Eckhaus instability. Continuous lines are guides for the eyes. Several subcritical transitions are indicated with green losanges. S, D and B stand for stationary, drifting and bistable regimes.

these paths involve two modes, respectively proportional to $\cos kx$ and $\sin kx$. Changing their relative amplitude corresponds to a neutral perturbation that shifts the pattern along x . A slight breaking of the $x \rightarrow -x$ symmetry induces a drift of the pattern at constant speed, *i.e.*, periodic reversals at instability onset instead of a stationary pattern. In the presence of lateral boundaries at $x = \pm L/2$, translational invariance is broken and other easy paths for reversals should be found. When L is such that patterns with $2n$ and $2n + 1$ half-wavelengths become simultaneously unstable, two modes with different parities with respect to the transformation $x \rightarrow -x$ are competing at the instability threshold [7]. Their interaction can describe wavelength changing instabilities, *i.e.* the Eckhaus instability [8]. When the $x \rightarrow -x$ symmetry is broken, a limit cycle involving these two patterns and the two ones with opposite polarities can be generated, thus describing periodic reversals. We present an experimental demonstration of this mechanism in the second section and a description of these observations in the framework of amplitude equations that govern the two modes with different parities in the third section. We show that these amplitude equations are similar to the ones that describe the reversals of the magnetic field in the VKS experiment [6]

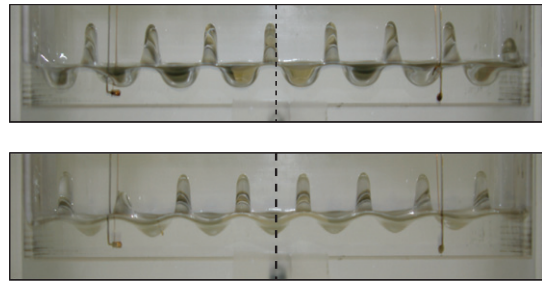


Fig. 2: (Color online) Snapshots of the experiment. The wave pattern contains (top panel) 8 wavelengths or (bottom panel) 8.5 wavelengths. The dotted line indicates the center of the cell.

and emphasize the similarities displayed by the trajectories of the reversals in both systems.

Experimental set-up and observations. – The experiment consists in parametrically forced subharmonic waves at the surface of a fluid. For parameters such that a nearly one-dimensional pattern is formed along, say, the x -direction, we investigate the effect of breaking the $x \rightarrow -x$ reflection symmetry. More precisely, the experiment consists in a rectangular cell of size $20 \times 4 \text{ cm}^2$ filled with a 10 mm deep layer of silicon oil. The oil viscosity is $100 \text{ mm}^2 \cdot \text{s}^{-1}$ and its density 0.965. We denote as x the direction parallel to the largest side of the cell and y the transverse one. The cell is shaken vertically along z with an acceleration $A_v \sqrt{2} \cos(\omega t)$ and horizontally in the x -direction with an acceleration $A_h \sqrt{2} \sin(\omega t + \phi)$. The vibration thus breaks the $x \rightarrow -x$ symmetry. Two capacity probes located symmetrically 60 mm away from the cell center measure the fluid height as a function of time. The system temperature is maintained fixed, close to $27.5 \text{ }^\circ\text{C}$, up to fluctuations of less than $0.1 \text{ }^\circ\text{C}$.

Unless otherwise stated, we focus on experiments performed with $\omega/(2\pi) = 18 \text{ Hz}$ and $\phi = 0^\circ$. As presented in fig. 1, the parameter space in the plane (A_h, A_v) is quite rich. A first instability is observed for a vertical acceleration $A_{vc} \simeq 0.85g$, roughly independent of the horizontal vibration. For $A_v \geq A_{vc}$, the flat surface is unstable and subharmonic waves form through the Faraday instability [9]. At onset, the pattern appears as 16 extrema aligned along the x -direction. Neighbouring peaks oscillate in phase opposition and the pattern thus contains eight wavelengths, as displayed in fig. 2. Note that in the transverse (y) direction, it contains only half a wavelength, *i.e.* only one peak, so that the system is essentially one dimensional. For small amplitude of the horizontal vibration, the pattern reaches a fixed position in the cell after the initial growth. At larger amplitude of the horizontal vibration, the same spatial structure forms but it is not steady. A schematic diagram of the pattern is presented in fig. 3. For simplicity, we consider a small number of wavelengths, and harmonic waves. Periodically in time, one peak appears at a side of the cell and the pattern temporarily contains 17 peaks, *i.e.*, 8.5 wavelengths, as displayed in fig. 2; this corresponds to $A \rightarrow B$ and $C \rightarrow D$

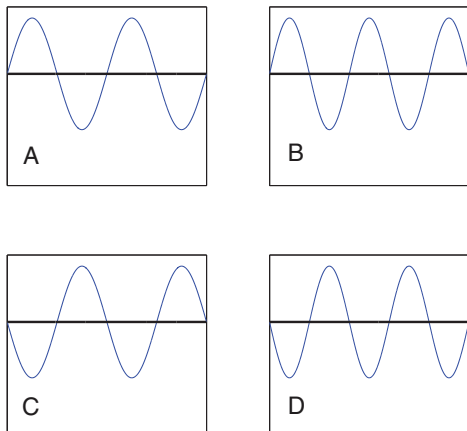


Fig. 3: (Color online) Simplified schematic diagram of the wave pattern. We consider only 2 or 2.5 wavelengths in the cell. From A to B and C to D, a peak appears on the right-hand side. Another peak disappears on the left-hand side from B to C and D to A. From A to C or B to D, the pattern is shifted by half a wavelength to the left, which corresponds to a sign change.

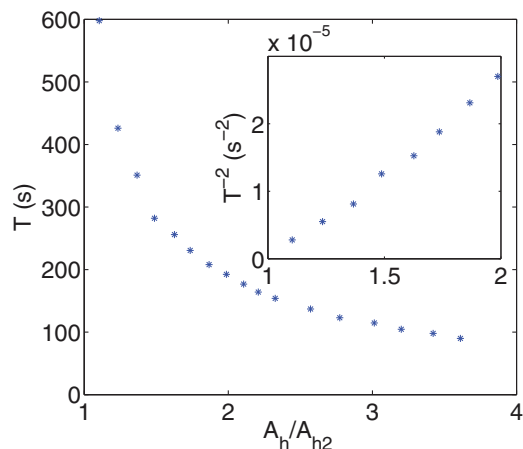


Fig. 4: (Color online) Period T of the unstable mode at the onset as a function of the horizontal vibration A_h/A_{h2} . T^{-2} close to the onset is displayed in the insert.

in the schematic. Later on, one peak disappears on the opposite side and the system is back to the 16-peak state but has shifted by half a wavelength ($B \rightarrow C$ and $D \rightarrow A$). The exchange between these two spatial structures thus results in a periodic drift of the pattern in the x -direction. To determine the period we measure the wave amplitude. The subharmonic component of the fluid height can be written $h = \text{Re}[H(x, t) \exp(i\omega t/2)]$. Standard data treatment allows us to remove the oscillation at pulsation $\omega/2$ and extract the period T of the slowly varying wave amplitude. In fig. 4, we display the period T at onset of instability as a function of A_h . The period is larger than 60 s, *i.e.*, it is quite long compared to the wave period $4\pi/\omega \simeq 0.11$ s. Therefore, for the slow evolution of the pattern, the drift regime appears as being generated through a Hopf

bifurcation even though the invariance under time translation is broken by the forcing. This threshold for Hopf bifurcation meets the threshold for stationary bifurcation at a codimension-2 point [10], located at $A_{v2} \simeq A_{vc} \simeq 0.85g$ and $A_{h2} \simeq 0.08g$. In agreement with the codimension-2 phenomenology, the period behaves as $T^{-2} \propto A_h - A_{h2}$ as displayed in the inset of fig. 4 and as discussed below. We note that a drift transition has been reported for the pattern formed by the periodic fluidization of a granular layer. A similar dependence of the period on the distance to threshold has been measured [11].

Amplitude equations for reversals. – To investigate theoretically this codimension-2 bifurcation, we consider the Swift-Hohenberg equation as a model of pattern-forming instability and study the effect of several terms that break the $x \rightarrow -x$ symmetry. This family of models reads

$$\partial_t \psi = (\alpha - (\partial_{xx} + k_c^2)^2) \psi + NL(\psi) + SB(\psi), \quad (1)$$

where SB stands for symmetry-breaking terms and NL for standard cubic nonlinear terms built with ψ or its spatial derivatives. Both terms are assumed to conserve the $\psi \rightarrow -\psi$ symmetry. The equation has to be supplemented with boundary conditions. A convenient choice is for the field and its second derivative to vanish at the boundaries $x = \pm L/2$. To give examples of $SB(\psi)$, one can consider $\epsilon \partial_x \psi$ or $\epsilon f(x)\psi$ where f is an odd function of x . Analytical progress can be made when two modes are both close to onset. The two modes are $D = \sin(2n\pi x/L)$ and $Q = \cos((2n+1)\pi x/L)$ and, keeping only these two nearly neutral modes, the field is $\psi = d(t)D(x) + q(t)Q(x)$ (see footnote ¹). Close to the onset of instability, the normal form theory enables us to write amplitude equations for d and q . It is convenient to introduce $A = d + iq$ that satisfies

$$\dot{A} = \mu A + \nu \bar{A} + nl(A), \quad (2)$$

where $nl(A)$ are nonlinear terms. In the absence of symmetry-breaking terms, $\epsilon = 0$, the system is symmetric under reflection with respect to $x = 0$. We note that the two modes have opposite parities under this transformation: one is odd and the other one is even. Then the symmetry enforces the invariance of eq. (2) under $A \rightarrow -\bar{A}$. In other words, when the symmetry is not broken, the imaginary parts of μ and ν (say μ_i and ν_i) vanish. For small symmetry breaking and close to the onset of instability, all the coefficients can be calculated through a perturbative expansion in ϵ [12]. The coefficients μ_i and ν_i are proportional to the amplitude ϵ of the symmetry-breaking terms. In the limit of a large system, $n \gg 1$, a further simplification takes place: to lowest order in $1/n$ the nonlinear terms are proportional to

$$nl(A) = \eta (5A^2 \bar{A} - \bar{A}^3), \quad (3)$$

¹From the linear part of eq. (1), the two modes have same growth rate provided $2(k_c L)^2 = (2n)^2 + (2n+1)^2$. For k_c close to this value, by increasing α , the two modes become nearly marginal while the other modes remain stable and can be eliminated.

where η is a coefficient. We conclude from this calculation that, whatever the form of the symmetry-breaking and nonlinear terms in eq. (1), it can be reduced to eqs. (2) and (3) to describe the evolution of a large system subject to a weak symmetry breaking, in the vicinity of the instability threshold of two spatial modes. Nonlinear effects saturate the instability if the real part of the coefficient η is negative. In line with the experimental observations, we assume that this is the case.

Before using these equations to understand the experimentally observed regimes, we make some comments about their generality. As mentioned above, eq. (2) is valid provided the coefficient k_c in eq. (1) is tuned so that only two modes are simultaneously close to criticality. The range in α above criticality for which these two modes are the only unstable ones becomes narrower and narrower as $L \rightarrow \infty$. This approach to the large-domain limit was originally proposed by Knobloch and Guckenheimer [7], who considered the Boussinesq equations of thermal convection. Our model is an application of the same method to the Swift-Hohenberg equation, the additional ingredient being an external breaking of the reflection symmetry.

Another approach consists in deriving an amplitude equation for the complex amplitude Z at wave number k_c , using symmetry considerations. In the large-domain limit, one may assume that the nonlinear terms remain phase invariant, which leads to

$$\dot{Z} = \mu Z + \nu \bar{Z} + \gamma Z^2 \bar{Z}. \quad (4)$$

$\nu = 0$ corresponds to a layer of infinite horizontal extent, for which translational invariance imposes the invariance of eq. (4) to a phase shift of the complex amplitude Z . $\nu \bar{Z}$ is the leading-order term that takes into account that, although large, L is finite, so that translational invariance is broken. There is no constant term because the instability is subharmonic, which implies the invariance $Z \rightarrow -Z$ of eq. (4). Surprisingly, in the case of thermal convection, the assumption that the nonlinear terms are phase invariant is satisfied for periodic and for no-slip boundary conditions, but not for stress-free boundaries [13]. In the former cases, for large L the two eigenmodes look like pure sinusoidal patterns at wave number k_c in the bulk of the domain, the two modes being in quadrature: eq. (4) provides a good description of the system. By contrast, for stress-free boundaries the two first eigenmodes have different wavelengths, one of them having an extra half-wavelength inside the domain $[-L/2; L/2]$. Even in the large-domain limit, they cannot be written in the simple form $Z(t)e^{ik_c x}$; instead, the amplitude equation needs to be written in terms of a variable similar to A above. This amplitude equation appears to be invariant to the transformation $A \rightarrow i\bar{A}$, which leads to the two nonlinearities of (3) among the four possible cubic terms. In the presence of an external breaking of the $x \rightarrow -x$ symmetry, the coefficients of both amplitude equations are complex. Although A and Z are different amplitudes related to different descriptions of

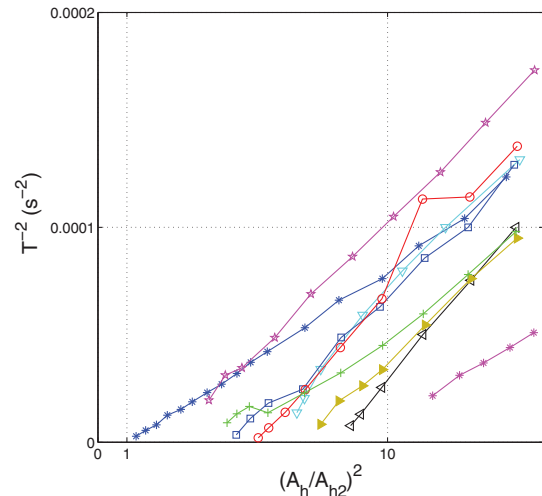


Fig. 5: (Color online) Square of the inverse of the period T^{-2} as a function of the square of the horizontal vibration $(A_h/A_{h2})^2$. Different values of the vertical acceleration are displayed, either at the onset of instability (blue $*$) $A_v/A_{vc} = 1$, or at least 6% above the onset (pink $*$) 1.06, (cyan ∇) 1.1, (black \triangle) 1.14, (yellow \blacktriangle) 1.18, (blue \square) 1.23, (red \circ) 1.27, (green $+$) 1.32, (magenta $*$) 1.36.

the linear problem, amplitude equations (2) and (4) lead to the same bifurcations of the zero solution if we consider that the nonlinear terms just saturate the amplitude.

Discussion of the experimental results. – We next focus on the different solutions of eqs. (2), (3). Transitions to unsteady regimes are observed when the symmetry is sufficiently broken: $|\mu_i|$ must be larger than $|\nu|$. At finite distance above the onset of instability, a time periodic behavior appears through a saddle-node bifurcation [10]. This is the drift regime. The period is easily calculated at linear order from eq. (2): $(2\pi/T) = (\mu_i^2 - \nu_i^2 - \nu_r^2)^{1/2}$, where ν_r is the real part of ν . In the first approximation, μ_i and ν_i are linear functions of the externally imposed symmetry breaking A_h . As can be seen in fig. 5, this prediction is verified by experimental data: T^{-2} appears to be linear in A_h^2 . Comparing the curve at onset (blue asterisks) to above onset, we observe that the nonlinear effects merely amount to a rescaling of the critical value of appearance of the drift with little change in the slope of T^{-2} as a function of A_h^2 . Note that in the vicinity of the codimension-2 point, other bifurcations than the saddle-node one are expected [10]. The domain over which these bifurcations exist is very narrow, and could not be clearly identified experimentally.

At zero horizontal vibration, another secondary instability is observed for a value of the vertical acceleration A_{ce} larger than A_{vc} . Above this value, the patterns are steady but bistable: depending on the initial conditions, two different states corresponding respectively to 16 or 17 peaks are observed. In other words, the state that is temporarily explored in the regime of drifting pattern is now stable. This bistability disappears for $A_v \leq A_{ce}$ and if

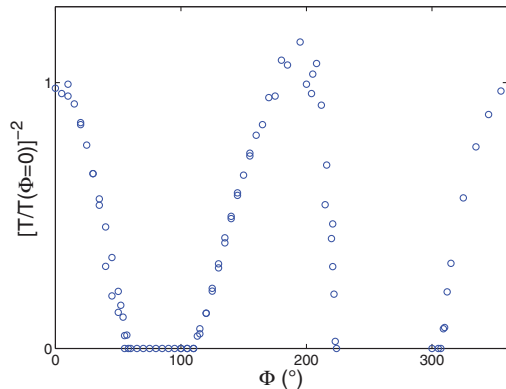


Fig. 6: (Color online) Square of the inverse of the period T^{-2} of the unstable mode as a function of the phase difference ϕ between the horizontal and vertical accelerations for $A_v/A_{vc} = 1.12$ and $A_h/A_{h2} = 3.75$.

the system is in the 17-peak state, it transitions abruptly toward the 16-peak state. This bifurcation is the Eckhaus instability [8]. We observe this phenomenon in the experiment and the transition line is shown (square symbols) in fig. 1. In eq. (1), the effect of symmetry breaking on the Eckhaus instability can be investigated theoretically. Generically, the onset of the Eckhaus instability is delayed by the symmetry-breaking terms, as observed experimentally [14].

For even larger values of the vertical acceleration (larger than $1.2g$), several bifurcations are observed. They involve subcritical transitions between modes that have different spatial structures in the transverse direction. The thresholds of these bifurcations appear as a complicated set of boundaries in the parameter space shown in fig. 1.

So far, we have considered only a given phase lag, $\phi = 0$. We can vary how the symmetry is broken by changing this phase ϕ between the two vibrations. The period of the drift is displayed in fig. 6 starting from parameters values for which drift occurs at $\phi = 0$. The period of the drift is strongly dependent on the phase. Saddle-node bifurcations to stationary regimes are observed and the pattern is steady for ϕ roughly between $\pi/3$ and $2\pi/3[\pi]$ (60 to 120°). Close to the threshold of the saddle-node bifurcations, we observe a linear dependence of T^{-2} on the phase, as expected. To conclude on the effect of the variation of the phase, we note that the phase selects the direction of propagation of the pattern. Expressed in terms of the motion of the container, the pattern moves horizontally in the same direction as the container moves when its vertical position is the lowest.

Finally, close to the saddle-node bifurcation, we expect the system to be sensitive to fluctuations. We have indeed observed that even temperature fluctuations can affect the dynamics. In particular, the period of the drift regime becomes random. We have quantified the effect of the fluctuations by adding noise to the horizontal vibration. The noise is low-pass filtered below a cut-off frequency of 40 Hz

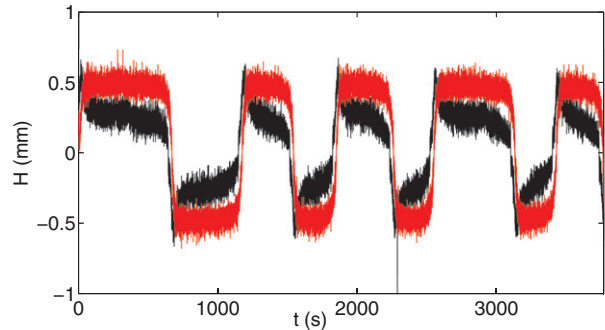


Fig. 7: (Color online) Time series of the pattern amplitude $H_{1,2}$ measured by the two probes when the horizontal acceleration is fluctuating. Random reversals are apparent. See text for details.

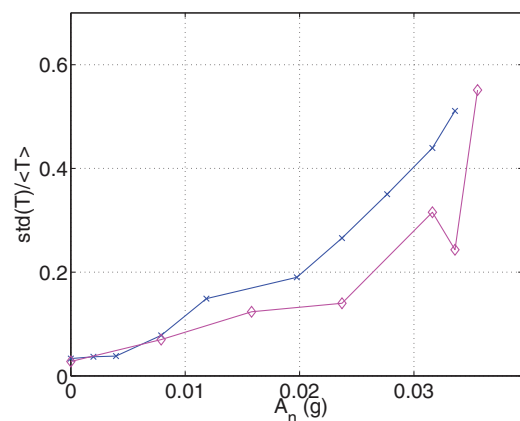


Fig. 8: (Color online) Relative fluctuations of the period $std(T)/\langle T \rangle$ as a function of the noise amplitude A_n for a vertical acceleration $A_v/A_c \simeq 1.02$ and a horizontal acceleration (blue \times): $A_h/A_{h2} \simeq 1.13$ (magenta \diamond): $A_h/A_{h2} \simeq 1.21$.

so that we can efficiently amplify the acceleration. This colored noise of standard deviation A_n adds incoherent fluctuations to the periodic vibration and, with a good approximation, the variance of the acceleration is the sum of A_n^2 and of the variance of the periodic acceleration.

In fig. 7, we plot the signed amplitude of the height $H_{1,2}$ measured by the capacity probes². As expected the drift becomes more and more random as A_n increases. The duration T between zeros of the wave amplitude fluctuates. The standard deviation over the mean, $std(T)/\langle T \rangle$ is displayed in fig. 8. Values close to 60% are reached, which correspond to widely distributed values of T .

As described in the discussion of fig. 3, when the pattern drifts over half a wavelength, the field amplitude changes sign, *i.e.*, the field reverses. The time series displayed in fig. 7 thus correspond to random reversals of the wave amplitude. We now understand why they strongly resemble those of magnetic-field reversals (see [6]

²The pattern being subharmonic, it has two possible phases with respect to the excitation. Positive values of the signed amplitude correspond to one of the phases and negative ones to the other phase.

for a comparison between magnetic-field reversals in several systems). Indeed, both systems correspond to field reversals generated by the coupling between two modes due to a broken symmetry. As a consequence, the amplitude equation for two coupled magnetic modes is the same as eq. (2). This explains the similarity between magnetic-field reversals and drifting patterns time series. In the VKS dynamo, and possibly for the geodynamo, reversals are induced by a symmetry breaking of the flow: the magnetic dipole drifts along its axis towards one boundary, while a dipole of the opposite polarity nucleates at the other boundary. This drift leads transiently to a quadrupolar magnetic structure, before the newly created dipole invades the entire fluid volume. As shown in this experiment, two modes with different parities with respect to a symmetry transformation thus provide an easy path for reversals in the phase space of the system when this symmetry is broken.

This work is supported by ANR-12-BS04-0005-02 and CNES.

REFERENCES

- [1] MOFFATT H. K., *Magnetic Field Generation in Electrically Conducting Fluids* (Cambridge University Press) 1978.
- [2] BALDWIN M. P. *et al.*, *Rev. Geophys.*, **39** (2001) 179.
- [3] BREUER M. and HANSEN U., *EPL*, **86** (2009) 24004; SUGIYAMA K. *et al.*, *Phys. Rev. Lett.*, **105** (2010) 034503; PAUL S. *et al.*, *Pramana J. Phys.*, **74** (2010) 75.
- [4] SOMMERIA J., *J. Fluid Mech.*, **170** (1986) 139; GALLET B. *et al.*, *Geophys. Astrophys. Fluid Dyn.*, **106** (2012) 468; MISHRA P. *et al.*, *Phys. Rev. E*, **91** (2015) 053005; HERAULT J. *et al.*, *EPL*, **111** (2015) 44002.
- [5] BERHANU M. *et al.*, *EPL*, **77** (2007) 59001.
- [6] PÉTRÉLIS F. and FAUVE S., *J. Phys.: Condens. Matter*, **20** (2008) 494203; PÉTRÉLIS F. *et al.*, *Phys. Rev. Lett.*, **102** (2009) 144503.
- [7] KNOBLOCH E. and GUCKENHEIMER J., *Phys. Rev. A*, **27** (1983) 408.
- [8] TUCKERMAN L. S. and BARKLEY D., *Physica D*, **46** (1990) 57.
- [9] FARADAY M., *Philos. Trans. R. Soc. London*, **121** (1831) 319.
- [10] GUCKENHEIMER J. and HOLMES P., *Nonlinear Oscillations, Dynamical Systems and Bifurcations of Vector Fields* (Springer-Verlag) 1986.
- [11] GARAY J. *et al.*, *Phys. Rev. E*, **85** (2012) 035201.
- [12] GALLET B., *Dynamique d'un champ grande échelle engendré sur un fond turbulent*, PhD Thesis, Ecole Normale Supérieure, 2011.
- [13] HIRSCHBERG P. and KNOBLOCH E., *J. Nonlinear Sci.*, **7** (1997) 537.
- [14] Drifting patterns involving two modes with different parities have been shown to occur in axisymmetric convection patterns: TUCKERMAN L. S. and BARKLEY D., *Phys. Rev. Lett.*, **61** (1988) 408; SIGGERS J. H., *J. Fluid Mech.*, **475** (2003) 357. The broken symmetry results from the local curvature of the convection rolls.